# Investigating the performance of square ring under uniform squeeze rate and internal pressure

## Untersuchung der Leistungsfähigkeit eines viereckigen Rings unter gleichförmiger Quetschrate und Innendruck

B.O. Alunda[1], D.O. Agumba[2], I.O. Ondicho[3], L.O. Otieno[3], M. Chepkoech[4], N.A. Mutua[5], J.S. Hawong[6]

Transportation and controlling fluid flow under high pressures in pumps, valves, boilers and heat exchangers is a common exercise in the industries. The main challenge, however that has confronted designers and manufacturers of pumps and valves along with those responsible for the maintenance and upkeep of such types of machinery is managing leakages at the positions where the seals are used. One fundamental feature of seal packing is the ability of the seal to 'flow' into the groove spaces and effectively block fluid from passing through them. The square ring has shown good 'flow' behavior in addition to offering low contact stresses. This research seeks to investigate the performance of the square ring. The Hertz contact theory and photoelastic experimental hybrid method are used in the study of the performance of the square ring under a squeeze rate of 20 % and varying internal pressure. It was observed that while increasing the applied internal pressure, the deformation length and angle increased due to the high stresses produced by the applied pressure. Additionally, was initiated at an internal pressure of 0.98 MPa.

**Keywords:** Square ring **/** photoelastic experimental hybrid method **/** stress components **/** isochromatic fringe patterns **/** internal pressure

**Schlüsselwörter:** Viereckiger Ring **/** photoelastische experimentelle Hybridmethode **/** beanspruchte Bauteile **/** isochromatische Streifenmuster **/** Innendruck

## 1 Introduction

Square ring seals have been used for many years as packing elements in high-pressure vessels such as ships, aircraft, and train parts especially for axial static applications (face seals) where the squeeze is applied to the top and bottom surfaces. Such locomotives are very crucial and can lead to the loss of many lives in case there is any failure. Unfortunately, in many design considerations of such

[1] Taita Taveta University, School of Mines and Engineering, 635-80300, VOI, REPUBLIC OF KENYA
[2] Machakos University, School of Mechanical and Manufacturing Engineering, 136-90100, MACHAKOS, REPUBLIC OF KENYA
[3] Dedan Kimathi University of Technology, School of Engineering, 657-10100, NYERI, REPUBLIC OF KENYA
[4] Howard University, School of Engineering and Architecture, 2300 6Th Street NW, WASHINGTON DC, UNITED STATES OF AMERICA
[5] Silla Entech Co. Ltd, R&D Institute, 41753, DAEGU, REPUBLIC OF KOREA
[6] Yeungnam University, School of Mechanical Engineering, 6200-00200, GYEONGSAN, REPUBLIC OF KOREA

Corresponding author: B.O. Alunda, Taita Taveta University, School of Mines and Engineering, 635-80300, VOI, REPUBLIC OF KENYA,
E-Mail: benard.ouma@ttu.ac.ke

© 2020 Wiley-VCH GmbH 

systems, the subjects of seals are often ignored partially because they represent the least expensive component of the system. In a pressure vessel, the joint is often the weaker member owing to the low modulus of elasticity of the seal. Besides, the combined stress acting on the seal is often complex and difficult to evaluate. Therefore, proper design considerations of the seals are required to minimize failures of the seals. One ideal method of understanding the stresses in the square ring is to test them in the actual service using photoelasticity which is based on a birefringent material that shows fringes when an external load is applied to it. When principles of photoelasticity are combined with stress freezing method, the complex model can be fabricated and loaded so that the deformations and the associated optical responses are locked into the three-dimensional model that can be analyzed later to obtain the interior stress information. Usually, the seals are made from a joint less homogenous material and thus easy to manufacture.

Seals with rectangular, circular and a combination of the two geometries have been studied in the past [1–5]. Of all the geometries mentioned, O-ring is the most popular shape; however, it is argued that the square rings have a wider contact area and therefore, more effective seal for static applications. Also, they are less expensive compared to any other sealing device and can be directly interchanged size for size with the O-ring. However, little information on the performance of the square ring and a combined loading of uniform squeeze rate and internal pressure is present. The geometric difference between the famous O-ring and square ring is that the cross-section of the latter has one more degree of freedom. The additional degree of freedom has the advantage of allowing the square ring to work in many applications as compared to an O-ring. Two such situations are a wide but shallow groove and a groove with one end higher than the other. The extra degree of freedom allows the thickness to vary, thus providing a better fit in the groove.

This research employs the photoelastic experimental hybrid method which combines the merits of analytical, experimental and numerical concepts to analyze the stresses in the seal [6, 7]. The hybrid technique of stress analysis has been developed by researchers [7–10]. In addition to analyzing the contact stresses in the square ring, the effects of extrusion on the performance and the dependence of the deformation angle on the applied internal pressure are investigated.

## 2 Basic theory

The stress components using Muskhelishvilli complex function and Airy stress function is shown in Equation 1 [11].

$$\begin{aligned}\sigma_y &= \mathrm{Re}\left[\, 2\phi'(z) + \bar{z}\phi''(z) + \psi'(z)\right],\\ \sigma_x &= \mathrm{Re}\left[2\phi'(z) - \bar{z}\phi''(z) - \psi'(z)\right],\\ \tau_{xy} &= \mathrm{Im}\left[\bar{z}\phi''(z) + \psi'(z)\right],\end{aligned} \tag{1}$$

where $z = x + iy$ and Re and Im are the real and the imaginary parts of the complex variable, respectively.

From Equation 1, the stress components have two complex functions $\phi(z)$ and $\psi(z)$. Therefore, if these two stress functions are known, the stress components can be easily determined.

### 2.1 Hertz contact theory

Generally, a contact problem is a half-plane problem. Thus, if the body occupies the lower portion of the body $S^-$ ($z < 0$), then an analytic complex function is defined by Equation 2 shown below [12];

$$\phi(\bar{z}) = -\bar{\phi}(z) - \bar{z}\bar{\phi}'(z) - \overline{\Psi(z)} \tag{2}$$

Replacing the variable z by $\bar{z}$ and assuming that z lies in $S^-$ (and hence $\bar{z}$ in $S^+$) and taking the complex conjugate values on both sides gives;

$$\Psi(z) = -\phi(z) + \bar{\phi}(z) - z\phi'(z) \tag{3}$$

Equation 3 is very important because it indicates the relationship between the stress function $\phi(z)$ and $\Psi(z)$.

Substituting Equation 3 into Equation 1, the stress equations in terms of only one function, $\phi(z)$ is obtained;

© 2020 Wiley-VCH GmbH 

$$\begin{aligned}\sigma_x &= \mathbf{Re}\left[3\phi(z) + \phi(\bar{z}) + z\phi'(z) - \bar{z}\phi'(z)\right]\\ \sigma_y &= \mathbf{Re}\left[\ \phi(z) - \phi(\bar{z}) - z\phi'(z) + \bar{z}\phi'(z)\right]\\ \tau_{xy} &= \mathbf{Im}\left[-\phi(z) - \phi(\bar{z}) - z\phi'(z) + \bar{z}\phi'(z)\right]\end{aligned} \tag{4}$$

As shown in Equation 4, by only determining the complex function $\phi(z)$, the stress components can be readily determined. The stress functions $\phi(z)$ and $\Psi(z)$ are analytic; thus, they can be expressed by a power series, as shown in Equation 5.

$$\phi(z) = \sum_{n=0}^{N} C_n z^{\frac{n}{2}} \tag{5.a}$$

$$\Psi(z) = \sum_{n=0}^{N} D_n z^{\frac{n}{2}} \tag{5.b}$$

Substituting Equation 5.a and Equation 5.b into Equation 3, the relative equation between the coefficients of the two stress functions $\phi(z)$ and $\Psi(z)$ is obtained, as shown in Equation 6.

$$D_n = -\frac{n}{2}C_n - \bar{C}_n \tag{6}$$

Using the stress functions $\phi(z)$ and $\Psi(z)$ and the relative equation between the coefficients of the two stress functions $\phi(z)$ and $\Psi(z)$, the stress components are obtained, as shown in Equation 7.

$$\begin{aligned}&\sigma_x =\\ &\sum_{n=1}^{N}\mathbf{Re}\left\{\begin{array}{l} C_n[2F(n\cdot z) - G(n\cdot z)]\\ +\overline{C}_n F(n\cdot z)\end{array}\right\}\\ &\sigma_y =\\ &\sum_{n=1}^{N}\mathbf{Re}\left\{\begin{array}{l} C_n[2F(n\cdot z) + G(n\cdot z)]\\ +\overline{C}_n F(n\cdot z)\end{array}\right\}\\ &\tau_{xy} =\\ &\sum_{n=1}^{N}\mathbf{Im}\left\{C_n G(n\cdot z) - \overline{C}_n F(n\cdot z)\right\}\end{aligned} \tag{7}$$

where

$$F(n\cdot z) = \frac{n}{2}\left\{\left(\frac{n}{2}-1\right)\bar{z} - \frac{n}{2}z\right\}z^{\left(\frac{n}{2}-2\right)}$$

and

$$G(n\cdot z) = \frac{n}{2}\left\{\left(\frac{n}{2}-1\right)\bar{z} - \frac{n}{2}z\right\}z^{\left(\frac{n}{2}-2\right)}$$

### 2.2 Photoelastic experimental hybrid method

The stress optic law for isotropic material is shown in Equation (8) below [13],

$$\left(\frac{N_f f_\sigma}{t}\right)^2 = (\sigma_x - \sigma_y)^2 + (2\tau_{xy})^2 \tag{8}$$

By combining the experimental and analytical values, an error is generated, which is never zero, and so a numerical method is used to calculate and minimize these errors. Thus, Equation 8 can be written as:

$$\left(\frac{N_f f_\sigma}{t}\right)^2 - (\sigma_x - \sigma_y)^2 - (2\tau_{xy})^2 = D(\varepsilon) \tag{9}$$

where $f_\sigma$ = Stress fringe value, $N_f$ = isochromatic fringe order, t = specimen thickness and z = position coordinates ($z = x + iy$).

When the precise experimental data are substituted into Equation 9, it becomes a function of only two (2) coefficients $a_n$ and $b_n$ of complex variable i.e. $C_n = a_n + ib_n$. Usually, a converging condition of $D(\varepsilon) \leq 10^{-5}$ is used because, at this point, the errors almost converge to zero. Applying numerical method to Equation 9 with the measured experimental data, $a_n$and $b_n$ are determined, which satisfies the limit values of errors [14].

Substituting Equation 7 into Equation 9, Equation 10 is obtained. $C_n = a_n + ib_n$ is then substituted into Equation 5.a and Equation 5.b to determine the stress functions $\phi(z)$ and $\Psi(z)$ for a given experimental condition. When these stress functions are substituted into the stress Equation 1, then the stress components at arbitrary load can be determined. The above procedures comprise the photoelastic experimental hybrid method for the contact stress analysis.

© 2020 Wiley-VCH GmbH 

$$D(\varepsilon) = \left(\frac{N_f f_\sigma}{t}\right)^2 - \left\{\begin{array}{l}\sum_{n=1}^{N} a_n \mathrm{Re}[2F(n\cdot z) - 2G(n\cdot z)] \\ + \sum_{n=1}^{N} b_n \mathrm{Im}[2F(n\cdot z) + 2G(n\cdot z)]\end{array}\right\}^2 - \left\{\begin{array}{l}\sum_{n=1}^{N} a_n \mathrm{Im}[2G(n\cdot z) - 2F(n\cdot z)] \\ + \sum_{n=1}^{N} b_n \mathrm{Re}[2G(n\cdot z) + 2F(n\cdot z)]\end{array}\right\}^2 \quad (10)$$

## 3 Experimental method

The square ring model made from aluminum was used to make the pink silicon mould owing to its ease of machinability, wide availability and cost-effectiveness [15], *Figure 1*a. The geometry of the square ring model had an internal diameter (ID) of 121.5 mm ± 0.1 mm and a cross-section of 6.98 mm ± 0.1 mm, Figure 1b.

A mould box was made from a cardboard box then the metallic square ring was placed inside and properly restrained. A pink silicon mould was prepared from an epoxy resin of Araldite (CY-230) and a hardener in a weight ratio of 10 : 3. The mixture was then poured into the mould box and allowed to solidify for about 12 hours before removal. Upon removal of the metallic ring, a cavity was left that had the dimensions identical to those of the square ring model required for the study. The prepared mould was placed inside the furnace for 12 hours. Two metallic tins were thoroughly cleaned and placed in the furnace to dry for about 30 min. Then the epoxy Araldite B41 and Hardener HT 903-1 were measured in the ratio of 10 : 3 by weight before pouring then inside two separate tins and heated for 2 hours at 120 °C in the furnace to melt. They were then mixed and stirred properly. The process was repeated three (3) times consecutively at a time interval of 5 mins to ensure that a homogeneous mixture is obtained. The mixture was then injected gently inside the mould cavity using a syringe. The setup was checked after 15 mins to remove any air bubbles then left in the furnace for 12 hours to polymerize (Araldite and Hardener) before to cooling to room temperature slowly while inside the furnace. The square ring made from the high-temperature epoxy resin was then taken out of the moulding box.

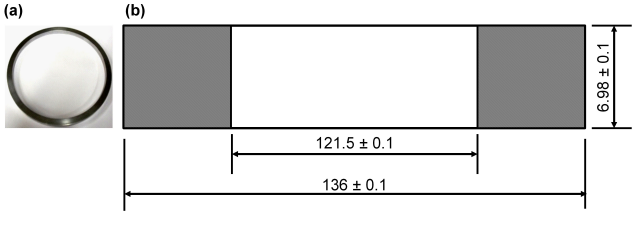


**Figure 1.** (a) Actual metallic square ring used to make the pink silicon mould, and (b) schematic of the cross-section showing the internal diameter and outer diameter of the ring. All dimensions are in mm.

Stress freezing process was carried out using experimental loading device. The cross-section of the experimental loading device is capable of giving a uniform squeeze rate and a varying internal pressure to the square ring, *Figure 2*a. The various squeeze rates are achieved by varying the internal diameter of the groove.

Additionally, the loading device has an opening at the top through which the internal pressure can be applied the valve used to maintain the pressure applied on the square ring, Figure 2b. The square

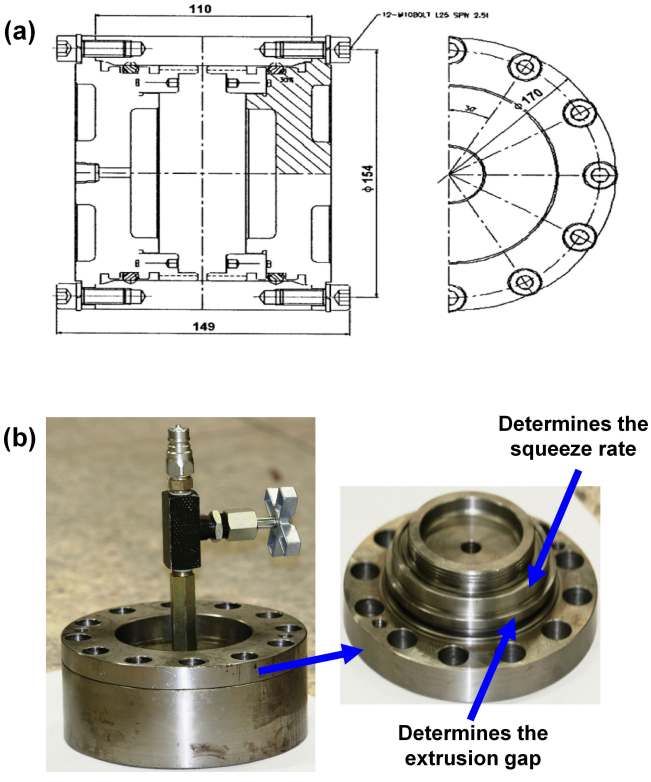


**Figure 2.** (a) The cross-section of the experimental loading device, and (b) The loading device designed to provide a uniform squeeze rate of 20 % and internal pressure.

© 2020 Wiley-VCH GmbH

ring was installed on the loading device then placed inside the stress freezing furnace following the stress freezing cycle, *Figure 3*.

After cooling to room temperature, the square ring was removed and sliced by using a band saw then polished appropriately to a thickness of less than 2 mm. The polished smooth slices were then put into the transparent glass container filled with a solution made from a mixture of α-bromonaphthalene and paraffin in the ratio of 1 : 0.585 by volume then placed appropriately on the transparent photoelastic experimental device, *Figure 4*. The device has a set of two quarter-wave plates, and the first quarter-wave plate is placed in between the polarizer and the specimen and the second quarter-wave placed between the specimen and the analyzer. The effect of adding the quarter-wave plate is to obtain circularly polarized light that produces only the isochromatic fringes without the isoclinic fringes. Therefore, eliminating the major difficulty of differentiating between the isoclinic fringe patterns and the isochromatic fringe patterns.

Photographs were taken for the isochromatic fringe patterns using a high-speed digital camera. The pictures obtained were transferred to the computer for image analysis.

The isochromatic fringes that were obtained from the experiment were used to generate graphic isochromatic using the already developed photoelastic experimental hybrid method. The generated isochromatic fringe patterns were compared to the actual isochromatic fringe patterns. When the regenerated isochromatic fringe patterns were not similar to the actual isochromatic fringe patterns, correctional steps were taken, and the analysis repeated until the two fringe patterns were similar or fit to a reasonable degree. Finally, the internal stresses were determined according to the photoelastic experimental hybrid method.

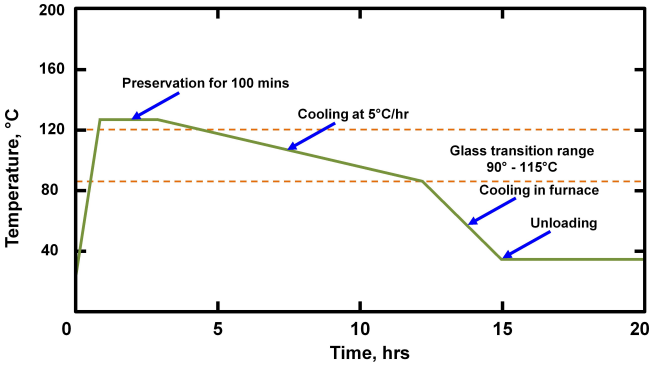


**Figure 3.** Stress freezing cycle

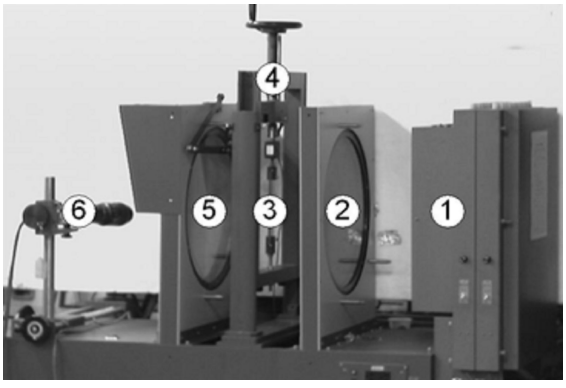


**Figure 4.** (1) – Light source, (2) – Polarizer and 1st quarter-wave, (3) – specimen, (4) – Loading device, (5) – Analyzer and 2nd quarter-wave (6) – CCD Camera. Schematic of transparent photoelastic experiment device

## 4 Experiment results and discussion

Photographs of the actual isochromatic fringe patterns of the square ring loaded under a uniform squeeze rate of 20 % and internal pressure, *Figure 5*. The images were obtained using a digital camera and the photoelastic experimental loading device, Figure 2. $P_i$ is the internal pressure that was

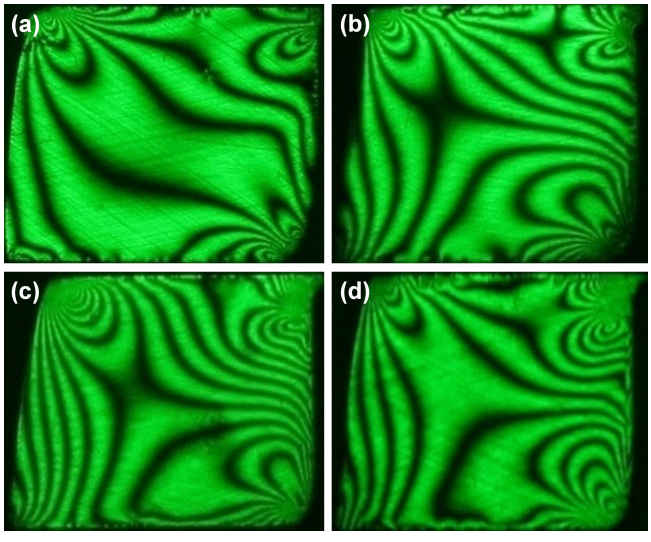


**Figure 5.** Actual isochromatic fringe pattern of the square ring under a uniform squeeze rate of 20 % and varying internal pressure: (a) $P_i = 0$ MPa, (b) $P_i = 0.98$ MPa, (c) $P_i = 1.96$ MPa and (d) $P_i = 2.94$ MPa.

© 2020 Wiley-VCH GmbH 

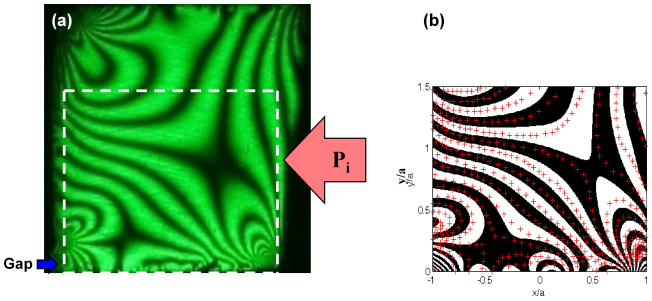


**Figure 6.** (a) Actual isochromatic, and (b) graphic isochromatic fringe patterns for the upper region of the square ring from the photoelastic experimental hybrid method (20 % squeeze rate, $P_i$ = 0.98 MPa and normalizing length, a = 3.167 mm)

applied to the square ring. It can be observed that an increase in the internal pressure leads to an increase in the intensity of the isochromatic fringe pattern up to an internal pressure of 1.96 MPa. Beyond 1.96 MPa, the intensity of the isochromatic fringe patterns decreased. There are very fewer isochromatic fringe patterns on the lower side of the square ring in all the 5 cases studied; therefore, no attention was paid to the lower side of the square ring. But the isochromatic fringe orders of the upper side and front side were much greater when the square ring was under uniform squeeze and internal pressure; thus, the upper region was carefully analyzed. The maximum intensity of the isochromatic fringe patterns when the internal pressure was 1.96 MPa could be as a result of the static friction between the steel metal and the epoxy at the beginning of extrusion that initiated at an internal pressure of 0.98 MPa. Leading to the accumulation of pressure in the groove. The static friction between the two materials depends on many factors such as

**Table 1.** Variation of deformation angle and extrusion length with internal pressure

| No. | Pressure (MPa) | Deformation angle (Ø) | Length (mm) |
|---|---|---|---|
| 1. | 0 | 4.018 | 0.418 |
| 2. | 0.98 | 4.481 | 0.454 |
| 3. | 1.96 | 4.718 | 0.501 |
| 4. | 2.94 | 6.947 | 0.716 |
| 5. | 3.92 | 7.125 | 0.740 |

Height = 5.963 mm

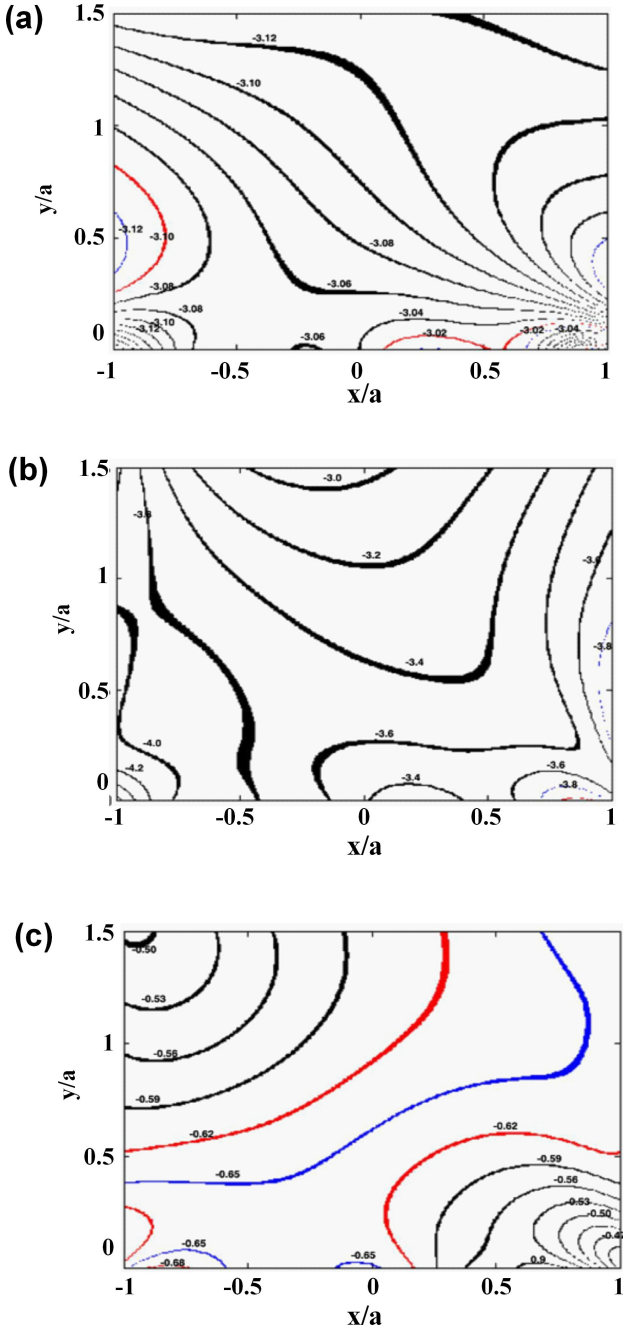


**Figure 7.** Normalized stress contours on the upper region of the square ring under a compression ratio of 20 % and an internal pressure of 0.98 MPa: (a) $\sigma_x$ ( = $\sigma_X/P_i$), (b) $\sigma_y$ ( = $\sigma_Y/P_i$), and (c) $\tau_{xy}$ ( = $\tau_{XY}/P_i$).

the pressure applied, surface finish (roughness), and limited displacement. The static friction greatly affects the performance of the square ring. The images of the isochromatic fringe patterns taken by the high-speed digital camera were loaded on the computer program for analysis.

© 2020 Wiley-VCH GmbH

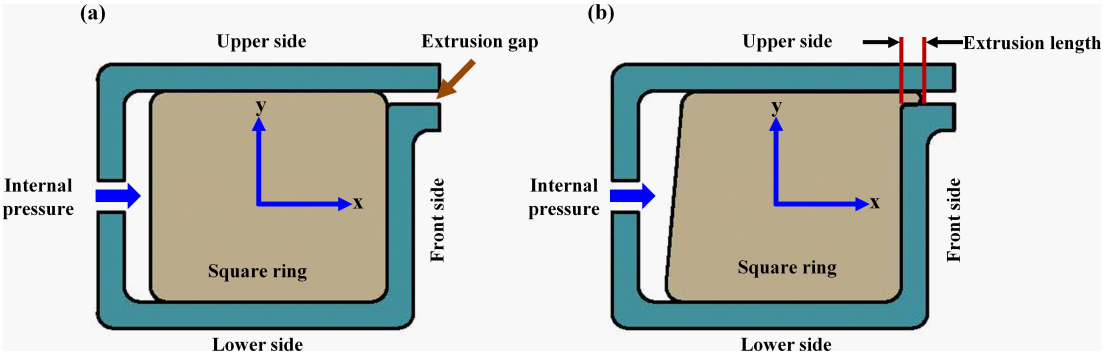


**Figure 8.** The loading conditions of the square ring; (a) before extrusion, and (b) after extrusion.

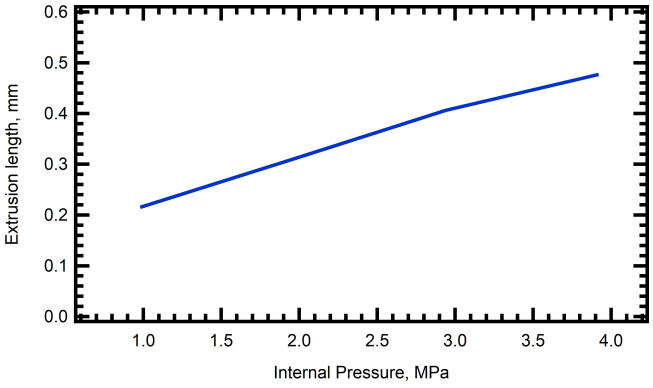


**Figure 9.** Graph showing the relationship between extrusion length and the internal pressure

The rectangular box (□) in the actual isochromatic fringe patterns represent the region from which the experimental data were collected. The cross marks "+" on the regenerated isochromatic fringe patterns show points from which the experimental data were collected. These points are located at almost along the centre line of the white and dark bands. The actual isochromatic fringe patterns and the regenerated isochromatic fringe patterns were compared and an error function adjusted until the two were similar, *Figure 6*

Additionally, the stress contours of the interior stress distribution of square ring under uniform squeeze rate of 20 % and the internal pressure of 0.98 MPa were also determined, *Figure 7*. The highest $\sigma_X$, $\sigma_Y$ and $\tau_{XY}$ internal stress values in these regions were 3.12 MPa, 4.2 MPa and 0.62 MPa respectively. Moreover, it was noted that the stresses on the upper part of the square ring have larger magnitudes compared to the contact stresses on the front and lower sides.

Extrusion of the square ring is defined as the pressure-induced distortion or extension of part of the seal into the clearance gap between mating seal surfaces. Normally this is experienced when the

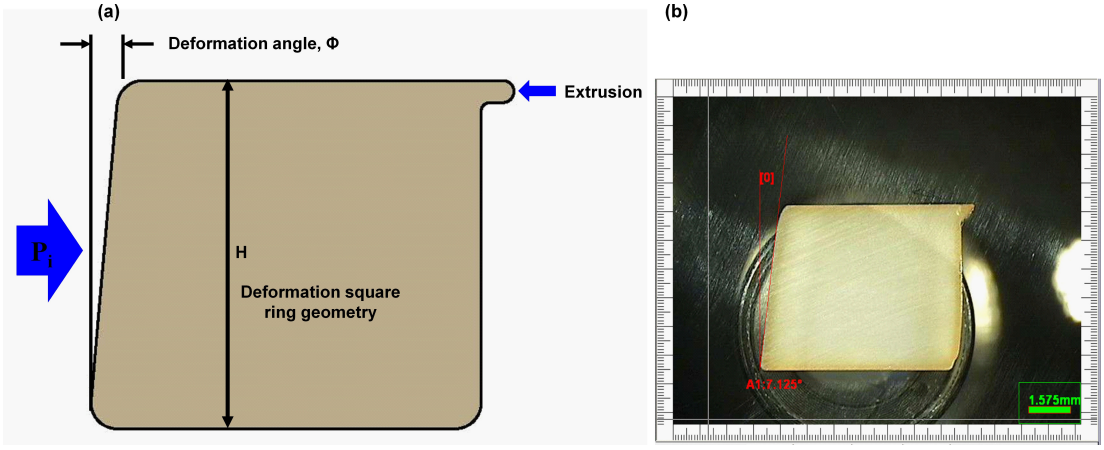


**Figure 10.** (a) Deformed geometry of the square ring under a uniform squeeze rate of 20 % and internal pressure, and (b) the deformed geometry of the square ring taken using the video microscope.

© 2020 Wiley-VCH GmbH 

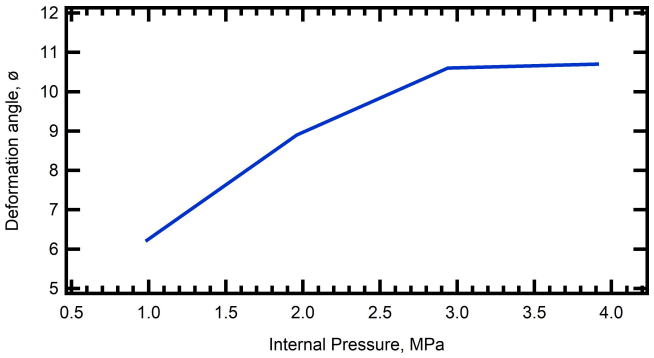


**Figure 11.** Graph showing the relationship between the deformation angle, Ø and the internal pressure of the square ring.

pressure of the fluid being contained exceeds the contact stress of the square ring; thus failure may occur when the contact stresses eventually exceed the yield strength of the square ring seal material.

The extrusion gap and extrusion length are important parameters in the study of square ring seals, *Figure 8*a, b. Due to the nature of the geometry of the ring, the extrusion under the compression ratio of 20 % occurred at very low pressures of 0.98 MPa, limiting the application of seals with a square geometry, especially for high-pressure applications. From earlier research done on O-ring under the same loading conditions, extrusion was found to occur when the internal pressure was above 3.92 MPa [8]. Therefore the O-ring may function better under high pressure when compared to the square ring.

With the use of the video microscope, we were able to measure the extrusion length of the square ring, and the results showed that the extrusion length of the square ring increases with an increase in the applied internal pressure, *Figure 9*. The extrusion length was measured to be 0.477 mm when the internal pressure was 2.94 MPa

The angle of deformation of the square ring under 20 % squeeze rate and internal pressure was also studied using the video microscope. It was observed that the deformation angle increased with internal pressure because of the stresses on the seal and the effects of extrusion. The internal pressure introduces more stresses and thus, larger deformation of the square ring. Larger deformations at higher pressure can also be attributed to the effect of extrusion since more material is forced into the extrusion gap.

The maximum deformation angle was found to be 7.125°, and it varied as a function of the internal pressure. *Table 1* shows the variation of the angle of deformation and the various internal pressures.

The extrusion phenomenon allows the elastomeric material to flow through the extrusion gap. An image of the square ring captured with a video camera showing the angle of deformation was measured, *Figure 10*b. Beyond the internal pressure of 2.94 MPa, the deformation stabilizes because there is no further flow of the material into the extrusion gap, *Figure 11*.

## 5 Conclusion

We have investigated the performance of a seal with the square geometry and found that extrusion initiated at a very low internal pressure of about 0.98 MPa. The region around the extrusion gap experienced relatively higher stress, and therefore failure is most likely to emanate from this position. The extrusion length was observed to vary with the internal pressure directly. Appropriate measures should be adopted to increase the pressure at which extrusion is initiated by using a superior rubber material model or a radiused square ring model. Alternatively, a combination of the two depending on the cost-effectiveness of the application can also be used. It was also found that the angle of deformation increased with internal pressure with the maximum value being 7.125°. We conclude that an increase in deformation implies a decrease in contact length on the upper side of the square ring, which affects the sealing properties or the packing ability of the square ring.

## Acknowledgement

This research was supported by Yeungnam University research grant 2012, Korea.

## 6 References

[1] B.R. Mose, J.-S. Hawong, J.H. Nam, *Mat.-wiss. u.Werkstofftech.* **2013**, *44*, 861.

© 2020 Wiley-VCH GmbH 

[2] B.R. Mose, D.K. Shin, D.C. Shin, *J Adv Mech Des Syst* **2017**, *11*, 17–00051.
[3] H.L. Johannesson, E. Kassfeldt, *Wear* **1989**, *130*, 3.
[4] B.R. Mose, J.S. Hawong, D.K. Shin, H.S. Lim, D.C. Shin, *J Mech Sci Technol* **2017**, *31*, 3657.
[5] G.E. Totten, *Handbook of Hydraulic Fluid Technology*, CRC Press, **2000**.
[6] S.T. Lin, R.E. Rowlands, *Opt Laser Eng* **1999**, *32*, 257.
[7] J.H. Nam, J.S. Hawong, S.L. Han, S.H. Park, *J Mech Sci Technol* **2008**, *22*, 2337.
[8] J.S. Hawong, J.H. Nam, S.L. Han, O.S. Kwon, G. Kwon, *J Mech Sci Technol* **2010**, *24*, 693.
[9] J.S. Hawong, J.H. Nam, S.L. Han, O. Kon, S. H. Park, *J Mech Sci Technol* **2009**, *23*, 2330.
[10] J.H. Nam, J.S. Hawong, D.C. Shin, B.R. Mose, *J Mech Sci Technol* **2011**, *25*, 2427.
[11] N.I. Muskhelishvili, *Some Basic Problems of Mathematical Theory of Elasticity*, 4th Edition, P. Noordhoff Ltd., Groningen Netherlands, **1963**.
[12] D.A. Hills, D. Nowell, A. Sackfield, *Mechanics of Elastic Contacts*, Butterworth-Heinemann, U.S.A. **1993**.
[13] R.C. Sampson, *Exp Mech* **1970**, *10*, 210.
[14] M.S. Bazaraa, C.M. Shetty, *Nonlinear Programming Theory and Algorithms*, John Wiley & Sons Inc. U.S.A. **1979**.
[15] B. Stojanovic, M. Bukvic, I. Epler, *Applied Engineering Letters* **2018**, *3*, 52.

Received in final form: April 23rd 2020

© 2020 Wiley-VCH GmbH 